NASA TECHNICAL NOTE

NASA TN D-3764

C.1

NASA TN D-3764

MEASUREMENT BY WAKE MOMENTUM SURVEYS AT MACH 1.61 AND 2.01 OF TURBULENT BOUNDARY-LAYER SKIN FRICTION ON FIVE SWEPT WINGS

by Russell B. Sorrells III, Mary W. Jackson, and K. R. Czarnecki

Langley Research Center
Langley Station, Hampton, Va.

NATIONAL AERONAUTICS AND SPACE ADMINISTRATION • WASHINGTON, D. C. • DECEMBER 1966

NASA TN D-3764

MEASUREMENT BY WAKE MOMENTUM SURVEYS AT MACH 1.61 AND 2.01 OF TURBULENT BOUNDARY-LAYER SKIN FRICTION ON FIVE SWEPT WINGS

By Russell B. Sorrells III, Mary W. Jackson, and K. R. Czarnecki

Langley Research Center
Langley Station, Hampton, Va.

NATIONAL AERONAUTICS AND SPACE ADMINISTRATION

For sale by the Clearinghouse for Federal Scientific and Technical Information
Springfield, Virginia 22151 – Price $2.00

MEASUREMENT BY WAKE MOMENTUM SURVEYS AT MACH 1.61 AND 2.01 OF TURBULENT BOUNDARY-LAYER SKIN FRICTION ON FIVE SWEPT WINGS

By Russell B. Sorrells III, Mary W. Jackson, and K. R. Czarnecki
Langley Research Center

SUMMARY

Momentum surveys were made in the wakes behind five semispan swept wings at Mach numbers of 1.61 and 2.01 to study the feasibility of this method of measuring the turbulent three-dimensional boundary-layer skin friction of the models. The wings had the same planform but employed various amounts of twist and camber. Transition was fixed and the free-stream Reynolds number, based on mean geometric chord, was 2.9×10^6 for both Mach numbers. The section skin-friction coefficients were calculated and the average skin-friction coefficient for the wing was compared with that obtained by the Sommer and Short T' flat-plate theory.

The results indicate that wake surveys can measure the viscous and separation momentum losses incurred by a swept wing with reasonable accuracy and that the viscous momentum losses can be related to section skin-friction coefficient with reasonable accuracy except when there is an appreciable amount of separation on the wing. It appears that for a high order of accuracy, wake surveys should be taken far enough downstream of the model to insure that the static pressure will be essentially constant through the wake at the particular spanwise station being surveyed. The integrated skin-friction values over the span are slightly greater than the integrated values from theory for the wings which had little or no flow separation. The cambered wings indicate values much greater than those obtained from theory because of a large amount of separated flow on the wings.

INTRODUCTION

Since the turbulent boundary-layer skin friction is a significant part of the total drag of a supersonic airplane, it is of interest to consider skin-friction distribution over the entire configuration as well as to investigate methods of reliably estimating its sum. Some measurements of the three-dimensional boundary-layer skin friction on hollow cylinders and axisymmetric bodies have been made by means of wake-survey techniques

(see refs. 1 to 3), but very few such measurements have been made on wings, wing-body combinations, or complete configurations.

The purpose of the present investigation was to study the applicability of the wake-survey technique to the measurement of the skin friction on lifting and nonlifting wings and to investigate the distribution of skin friction on such wings. The series of five wings had identical planforms and thickness distributions but employed various amounts of twist and camber. Surveys were made at Mach numbers 1.61 and 2.01, at angles of attack of -3°, 0°, 3°, and 6°, and at several spanwise stations. Transition was fixed and all tests were conducted at a free-stream Reynolds number, based on the mean geometric chord, of 2.9×10^6.

SYMBOLS

a	speed of sound; mean-line designation
b	wing span
c	local chord
$\bar{c}$	mean geometric chord, 10.33 inches or 26.24 centimeters
c_F	section skin-friction coefficient based on local chord and free-stream conditions
C_F	average wing skin-friction coefficient based on mean geometric chord, $\int_0^1 c_F \frac{c}{\bar{c}} d\left(\frac{y}{b/2}\right)$
M	Mach number
p	pressure
$p_{t,2}$	total pressure behind normal shock of probe
R_c	Reynolds number based on free-stream conditions and local chord
T	temperature
u	velocity

x axial distance downstream measured from wing trailing edge in percent local chord

y spanwise distance measured from root chord

$\frac{y}{b/2}$ semispan station

z vertical distance measured through wake arbitrarily referenced so that the (δ_l) point of the $p_{t,2}$ profile is located at $z = 0$

α angle of attack of wing root

γ ratio of specific heat at constant pressure to specific heat at constant volume (1.4 for air)

δ_u upper limit of skin-friction wake

δ_l lower limit of skin-friction wake

θ general two-dimensional wake momentum thickness, $\int_{\delta_l}^{\delta_u} \frac{\rho u}{\rho_\infty u_\infty}\left(1 - \frac{u}{u_\infty}\right)dz$

θ_F two-dimensional wake momentum thickness due to skin friction, $\theta - \theta_{W+A}$

θ_{W+A} two-dimensional wake momentum thickness due to combined effect of wave drag losses and momentum thickness change due to acceleration of flow at a given station, $\int_{\delta_l}^{\delta_u} \frac{\rho u}{\rho_\infty u_\infty}\left(1 - \frac{u_{W+A}}{u_\infty}\right)dz$

ρ density

Subscripts:

W+A conditions due to wave-drag and flow-acceleration effects which become fictitious between δ_l and δ_u

t total or stagnation conditions

∞ free-stream conditions

APPARATUS AND METHODS

Models and Model Mounting

Five semispan wings with the same planform but different surface shapes were tested. The planform and the various root sections are shown in figure 1. One wing had a flat mean surface (designated wing F), one was cambered (designated wing C), one was twisted (designated wing 1), one was cambered and twisted (designated wing 4), and one was reflexed and cambered (designated wing 5). These designations are consistent with previously used designations for these wings.

All the wings had an NACA 65A005 thickness distribution in the streamwise direction, 50° of sweepback of the quarter-chord line, a taper ratio of 0.20, and an aspect ratio of 3.5. The ordinates for the NACA 65A005 thickness distribution are given in reference 4. At each spanwise station in the streamwise direction, the cambered wing had an NACA a = 0 mean line modified to have a maximum height of 4 percent chord. (See page 93 of ref. 5 for unmodified mean line.) The twisted wing was derived from the flat wing by linearly rotating each spanwise station about the leading edge to a maximum value of 6° of washout at the tip. The cambered and twisted wing had at each spanwise station an a = 0 mean line modified to have a maximum height of 4 percent chord and was twisted in the same manner as was wing 1 with a linear spanwise twist variation having 6° of washout at the tip. The untwisted reflex cambered wing had a 1-wavelength sinusoidal mean line with a leading-edge angle of attack of -6°.

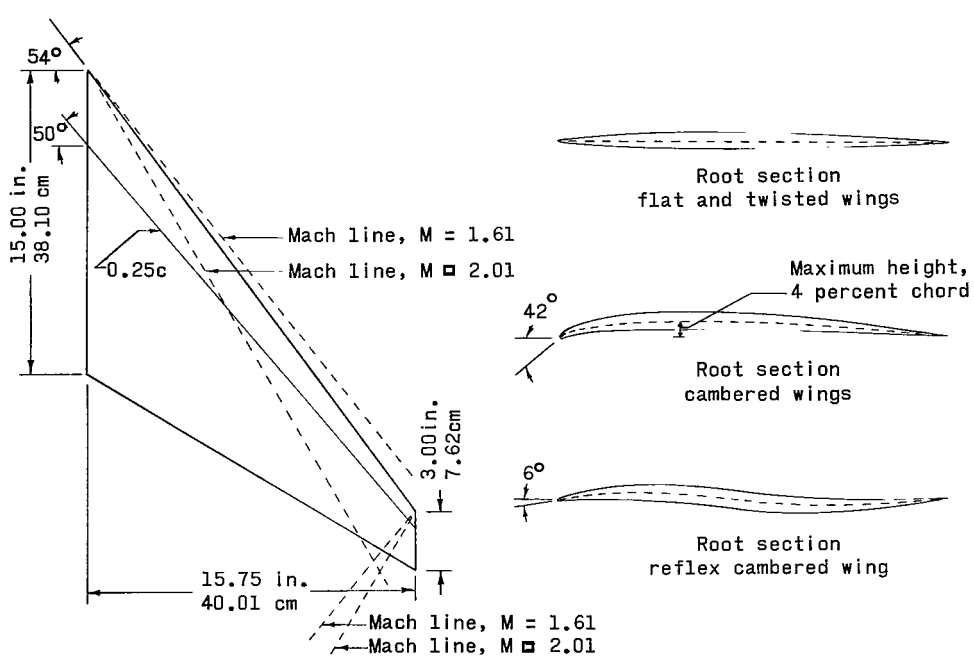

Figure 1.- Planform and various root sections of wings. (Sections not to planform scale.)

The semispan wings were mounted horizontally in the tunnel from a turntable in a boundary-layer bypass plate (fig. 2) which was located vertically in the test section about 10 inches (25.4 cm) from the tunnel wall.

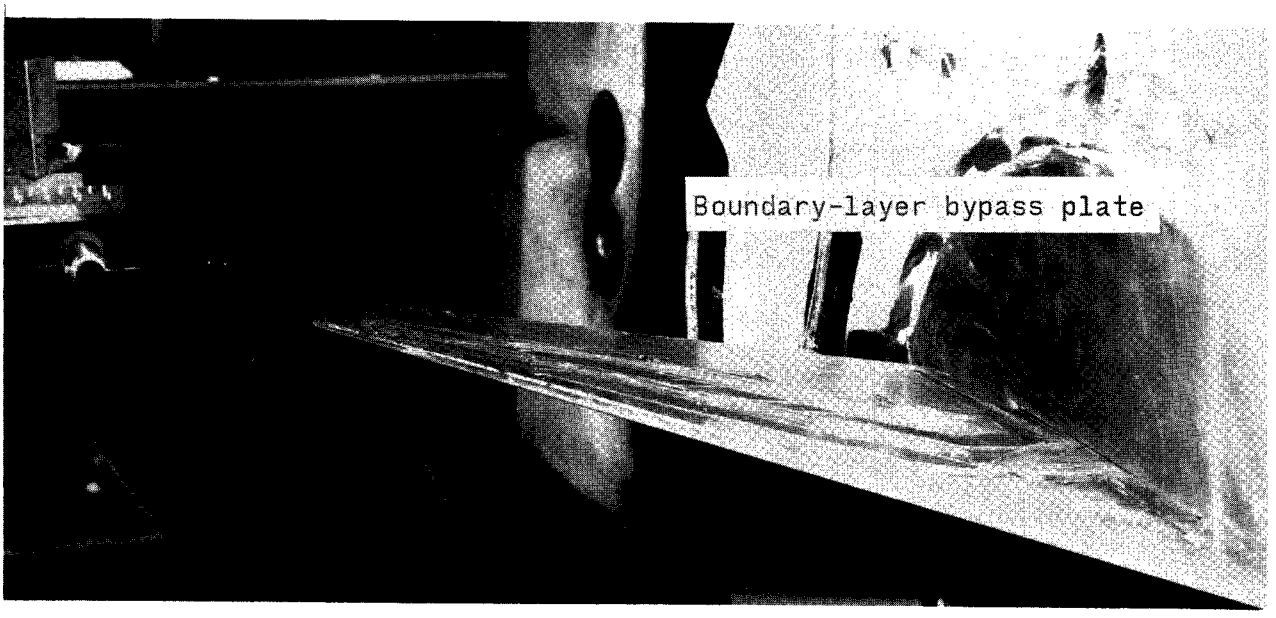

(a) Viewed from upstream. L-63-1335.1

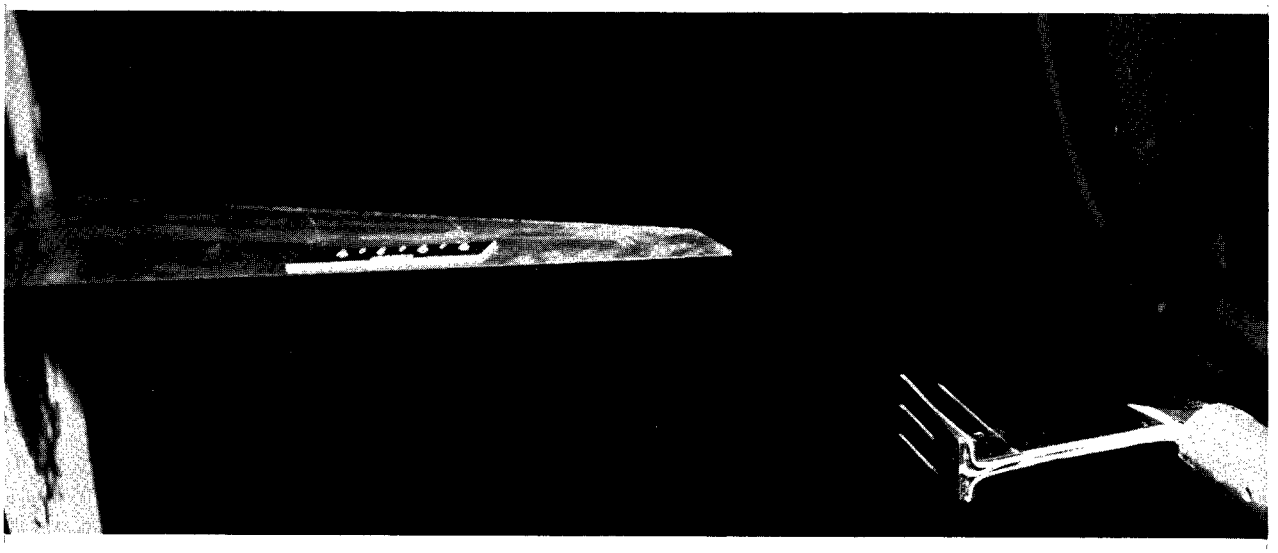

(b) Viewed from downstream. L-63-1334

Figure 2.- Photograph of test installation showing wing and movable rake.

Tests and Procedures

All tests were conducted in the Langley 4- by 4-foot supersonic pressure tunnel at a free-stream Reynolds number, based on the mean geometric chord, of 2.9×10^6 and at Mach numbers 1.61 and 2.01. The stagnation pressures were 11.8 and 14 psi (8.1 and 9.6 N/cm^2) for Mach numbers 1.61 and 2.01, respectively. The stagnation temperatures were 560° and 570° R (311° and 316° K) for Mach numbers 1.61 and 2.01, respectively.

Transition was fixed 1/2 inch (1.27 cm) from the wing leading edge by using No. 60 carborundum grains sparsely distributed over a 1/8-inch-wide (0.32-cm) band. Angle of attack was set by manual rotation of the turntable on which the models were mounted and was measured by a vernier scale outside the tunnel. Data were taken at angles of attack of -3°, 0°, 3°, and 6°.

Total- and static-pressure profiles were taken through the wake by means of a rake (fig. 2) composed of three total-pressure probes and one static-pressure probe. The rake was attached to an actuator which could be moved axially and vertically, and the actuator was mounted on the tunnel main sting which could be traversed across the tunnel. Consequently, the rake could be moved electrically in three directions from outside the tunnel. Figure 3 shows the various survey stations as well as Mach lines emanating from the root and tip leading edges of the wing. The locations of the various survey stations are given in table 1. Total- and static-pressure profiles were taken at seven stations for wings 1, 4, and 5; whereas, profiles were taken at six stations for wings F and C. These stations are located at the 25-percent-c position behind the wing; at station 2, however, additional profiles were taken at two other positions farther behind the wing as noted by the two cross marks in figure 3.

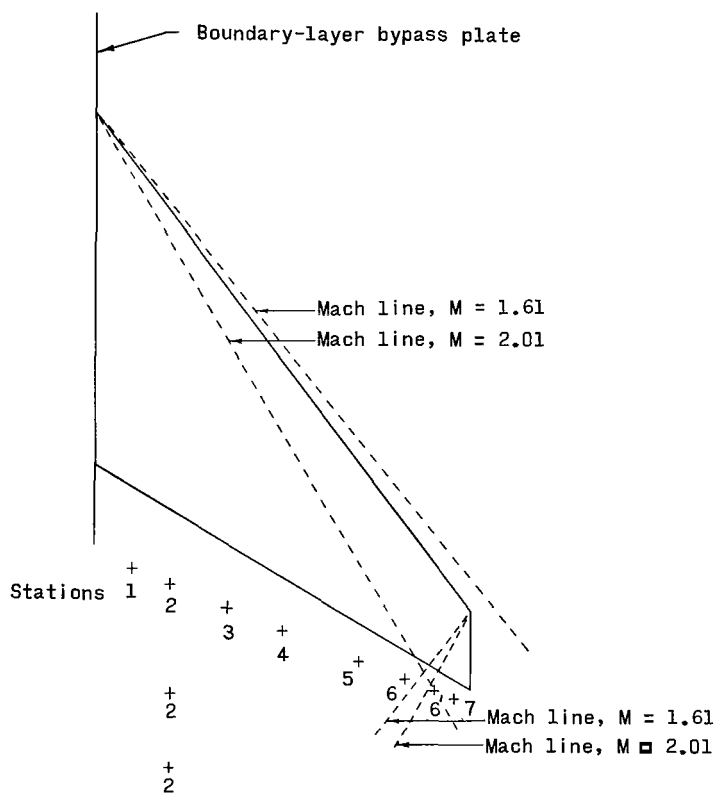

Figure 3.- Plan view of wing showing survey stations.

TABLE 1.- SEMISPAN LOCATION OF THE VARIOUS SURVEY STATIONS

[See fig. 3]

Wing	2y/b at station:						
	1	2	3	4	5	6 or 6'	7
				M = 1.61			
F	0.135	0.200	0.350	0.500	0.700	0.900	
1	.111	.200	.350	.500	.700	.825	0.950
C	.135	.200	.350	.500	.700	.900	
4	.113	.200	.350	.500	.700	.825	.950
5	.106	.200	.350	.500	.700	.825	.950
				M = 2.01			
F		0.200	0.350	0.500	0.700	0.900	
1	0.085	.200	.350	.500	.700	.825	0.950
C		.200	.350	.500	.700	.900	
4	.082	.200	.350	.500	.700	.825	.950
5	.084	.200	.350	.500	.700	.825	.950

Data Reduction

The section skin-friction coefficients were calculated from the equation

$$c_F = \frac{2\theta_F}{c} \tag{1}$$

where θ_F is the two-dimensional momentum thickness due to skin-friction losses and is obtained from the expression

$$\theta_F = \theta - \theta_{W+A} \tag{2}$$

where

$$\theta = \sum_{\delta_l}^{\delta_u} \frac{pM}{p_\infty M_\infty}\left(\sqrt{\frac{1+\frac{\gamma-1}{2}M^2}{1+\frac{\gamma-1}{2}M_\infty{}^2}} - \frac{M}{M_\infty}\right)\Delta z \tag{3}$$

and

$$\theta_{W+A} = \sum_{\delta_l}^{\delta_u} \frac{pM}{p_\infty M_\infty}\left(\sqrt{\frac{1+\frac{\gamma-1}{2}M^2}{1+\frac{\gamma-1}{2}M_\infty{}^2}} - \frac{M_{W+A}}{M_\infty}\sqrt{\frac{1+\frac{\gamma-1}{2}M^2}{1+\frac{\gamma-1}{2}M_{W+A}{}^2}}\right)\Delta z \tag{4}$$

(See appendices A, B, and C for the discussion and derivation of eqs. (2), (3), and (4).) The momentum thicknesses θ and θ_{W+A} are calculated from the static- and total-pressure profiles. Figure 4 shows some typical static- and total-pressure profiles. These included a profile showing the distortion effects caused by the tip vortex, a profile taken in an unseparated region, and two profiles showing the losses due to boundary-layer separation.

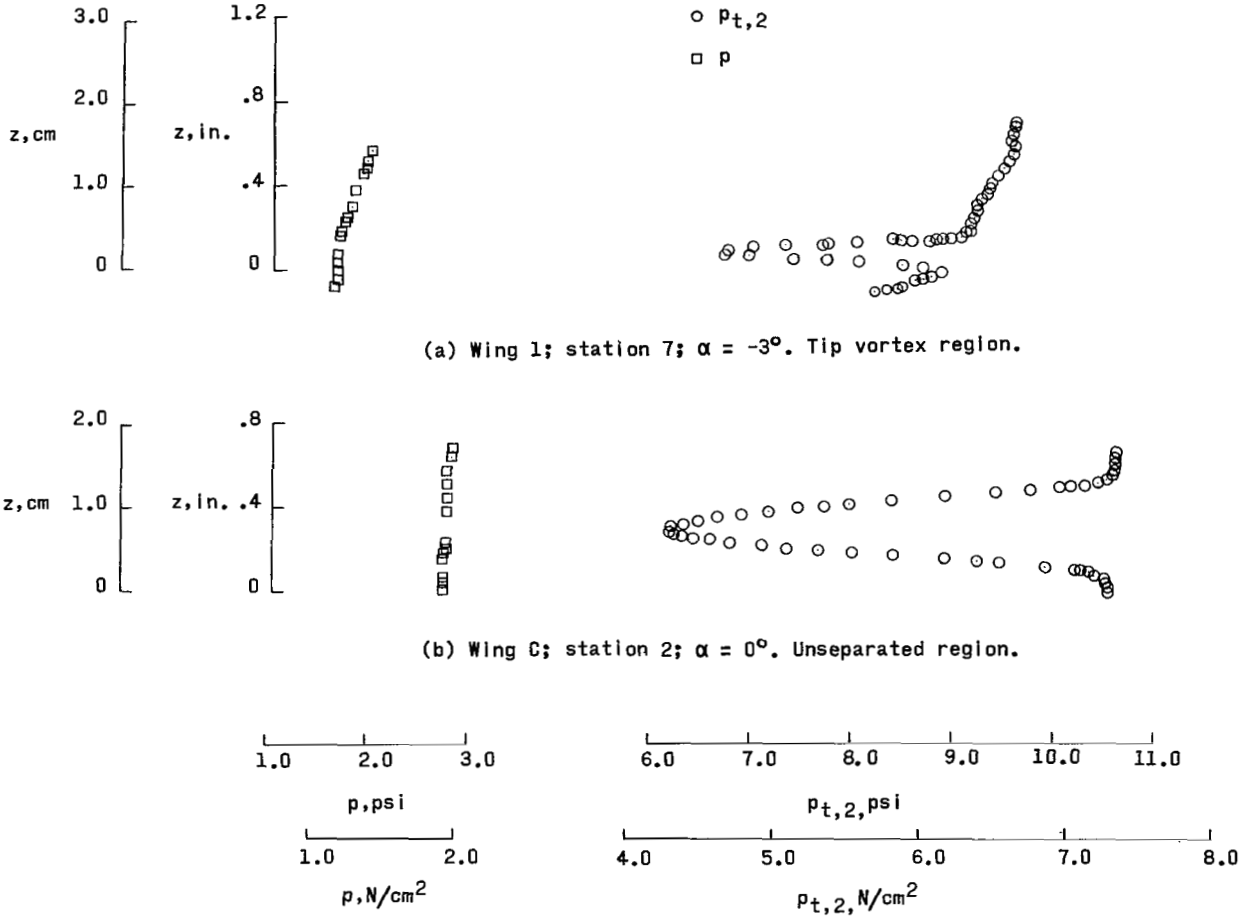

Figure 4.- Typical p and $p_{t,2}$ profiles. M = 1.61.

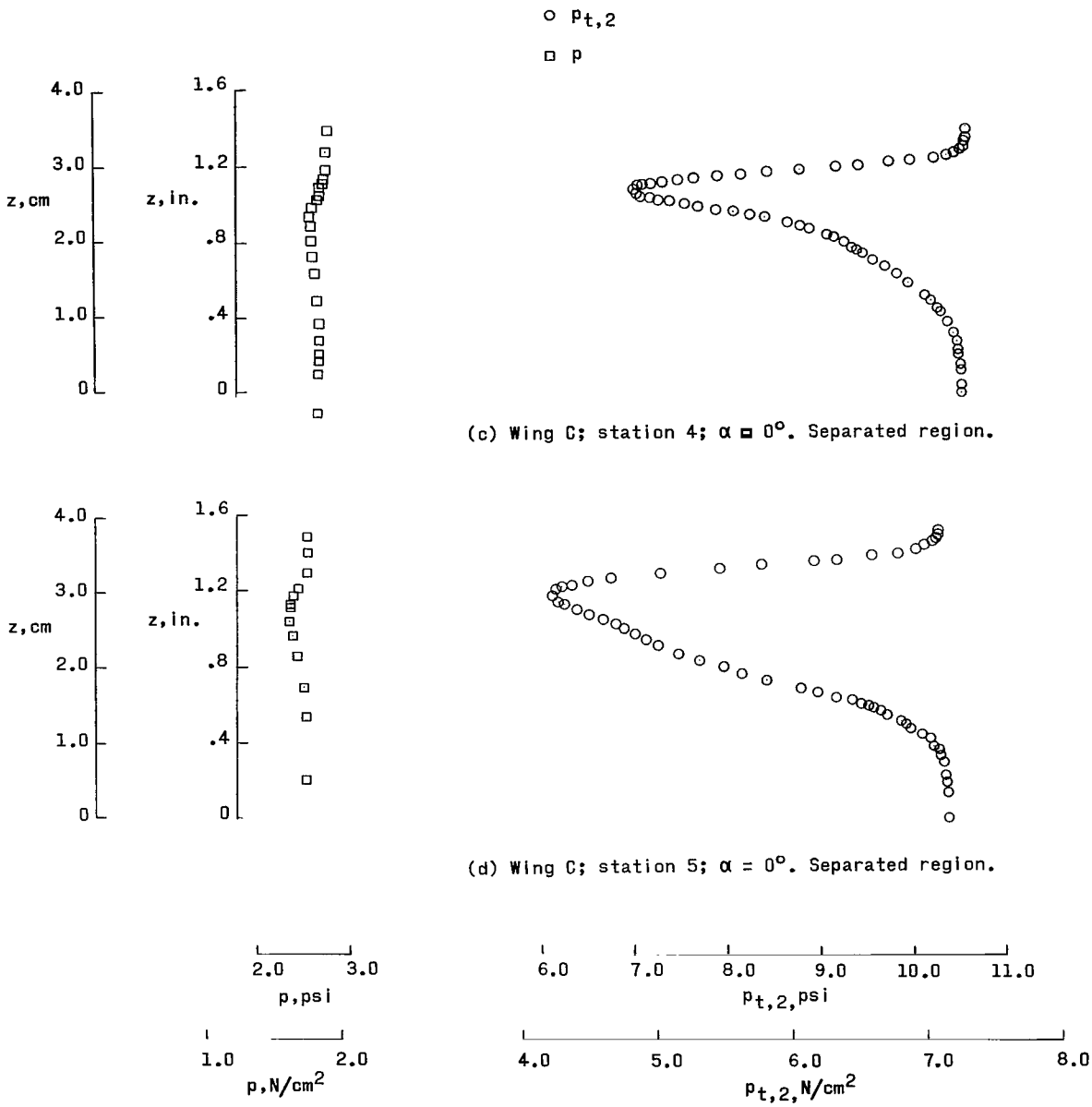

(c) Wing C; station 4; $\alpha = 0°$. Separated region.

(d) Wing C; station 5; $\alpha = 0°$. Separated region.

Figure 4.- Concluded.

RESULTS AND DISCUSSION

Section Skin-Friction Coefficients

The variation of the experimental section skin-friction coefficient based on mean geometric chord is presented for various spanwise stations and compared with the Sommer and Short T' flat-plate theory (ref. 6) in figures 5 and 6 for Mach numbers 1.61 and 2.01, respectively. The data curves generally were not faired through the most outboard measuring station. Instead, they were faired parallel to theory from the adjacent data point to the wing tip because the wing in a lifting condition would have a tip vortex (see ref. 7) that distorts the wake in the spanwise direction in the region of the most outboard measuring station and it is believed that the measurements in this region are not representative of the skin friction. Figure 4(a) illustrates the distortion effect of the tip vortex on a typical static- and total-pressure profile in the tip-vortex region. In order to avoid the boundary layer on the boundary-layer bypass plate, no wake surveys were made at the wing root; however, the data curves in figures 5 and 6 were also faired parallel to theory from the most inboard measuring station to the root of the wing.

Wing F.- The measured skin-friction values for wing F are slightly higher than those determined from theory and there is a tendency, especially at Mach number 2.01, for the skin-friction values to exceed the theory by a greater extent at the inboard stations than at the outboard stations. (See figs. 5(a) and 6(a).) This effect could have resulted from two causes. First, since the transition strip was equidistant from the leading edge across the entire span, the outboard stations have laminar flow over a greater percentage of the chord; and second, since the average section Mach number tends to be higher at the outboard stations, as indicated by reference 8, lower skin-friction coefficients would result.

At Mach number 1.61, wing F shows an increase in skin-friction coefficient at $\alpha = 6^{\circ}$ over that obtained at the other two angles of attack. (See fig. 5(a).) However, it is believed that the boundary layer is beginning to separate at the trailing edge and the increased momentum loss at $\alpha = 6^{\circ}$ is due to separation losses and not to an increase in skin-friction coefficient with angle of attack. Inasmuch as these momentum losses due to separation appear in the skin-friction wake, they will be included in the calculation of θ_F. Separation can result at moderate angles of attack because of the pressure rise at the trailing edge due to the flow on the upper surface of the wing having to negotiate the angle of recompression at the trailing edge. The possibility of separation at Mach number 1.61 is indicated in references 9 and 10 inasmuch as the pressure rise through the recompression at the trailing edge is estimated to be of sufficient magnitude to cause separation. The pressure rise was found for the given component of the local Mach

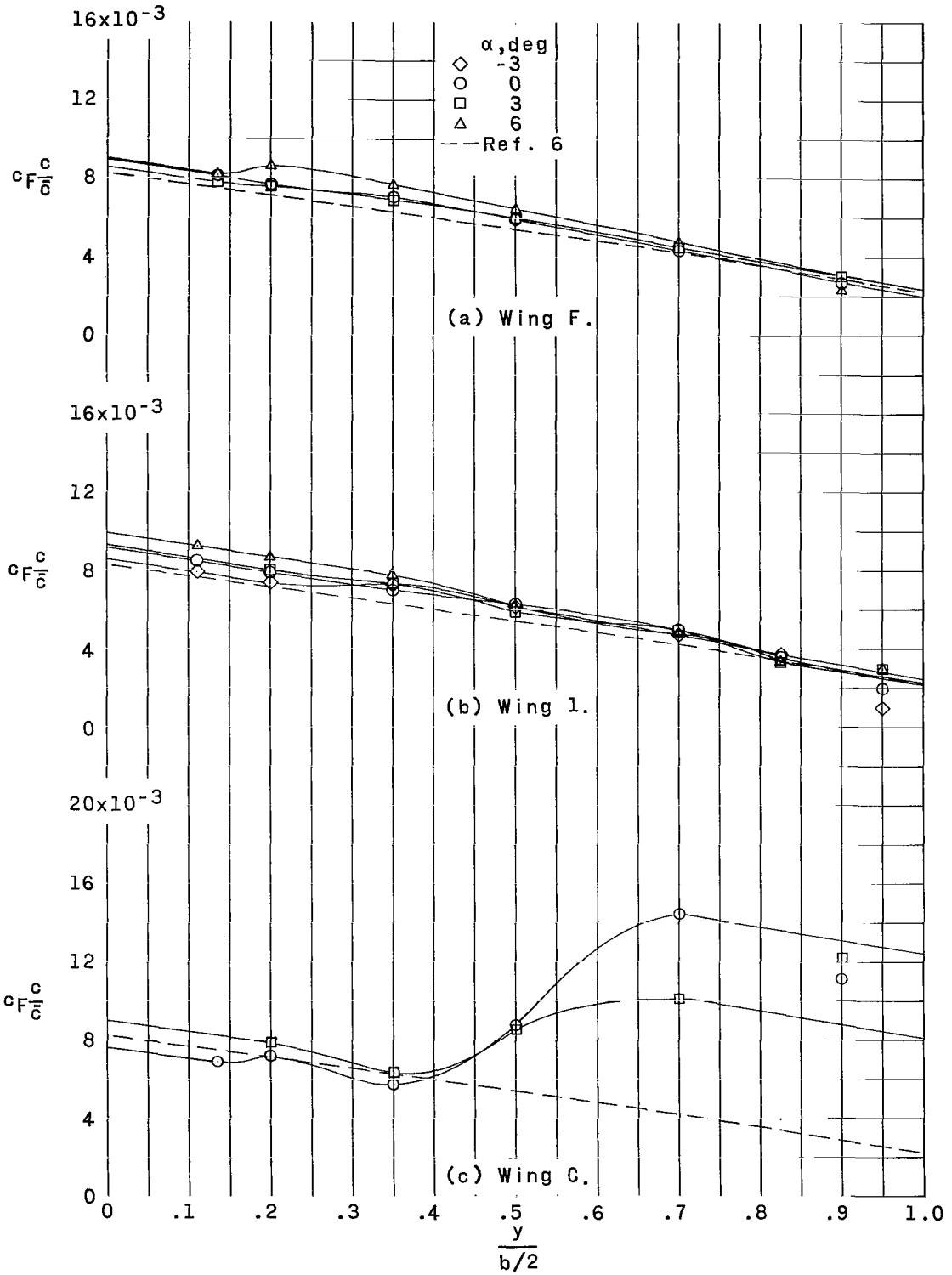

Figure 5.- Variation of section skin-friction coefficient based on $\bar{c}$ with semispan station. M = 1.61.

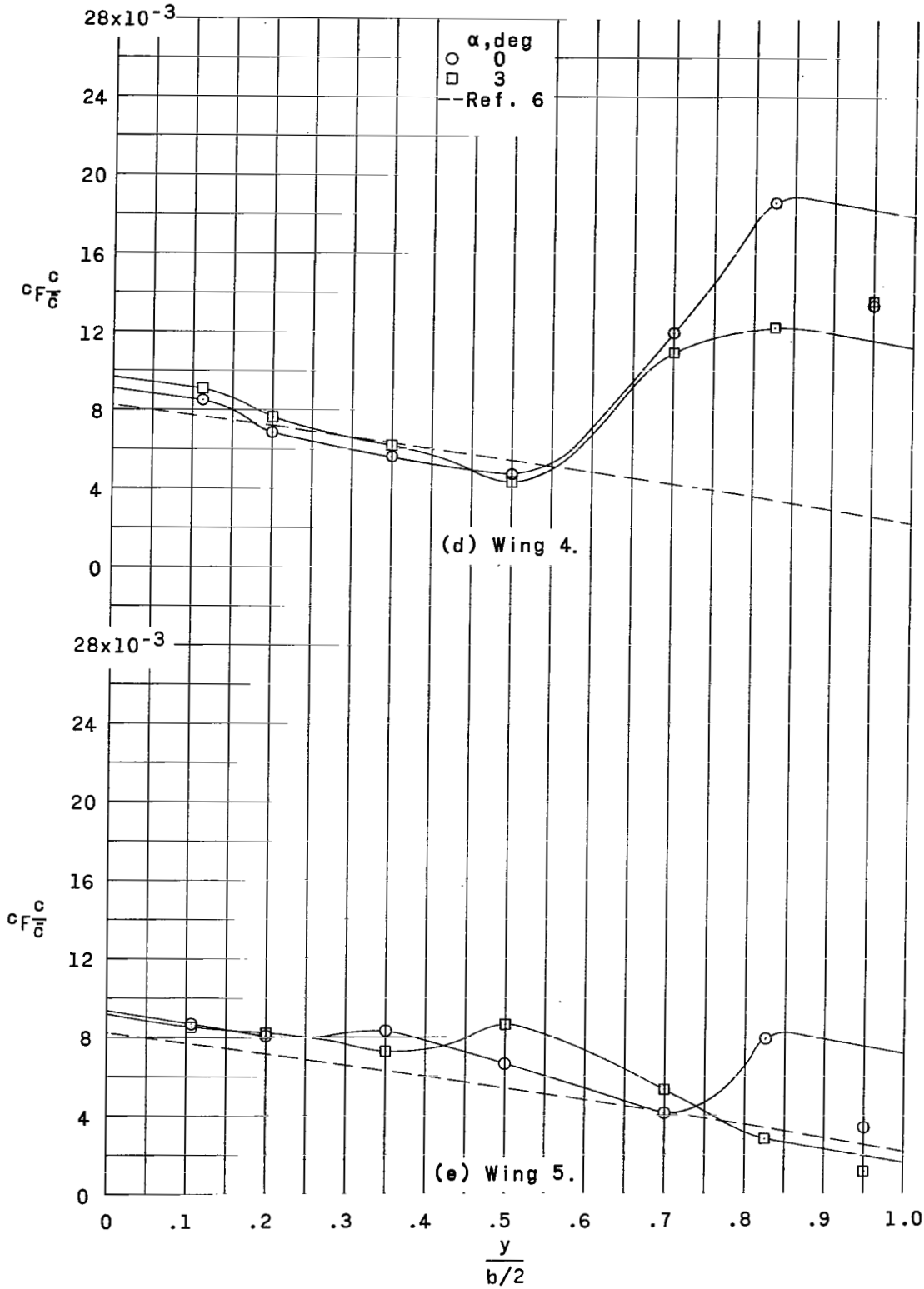

Figure 5.- Concluded.

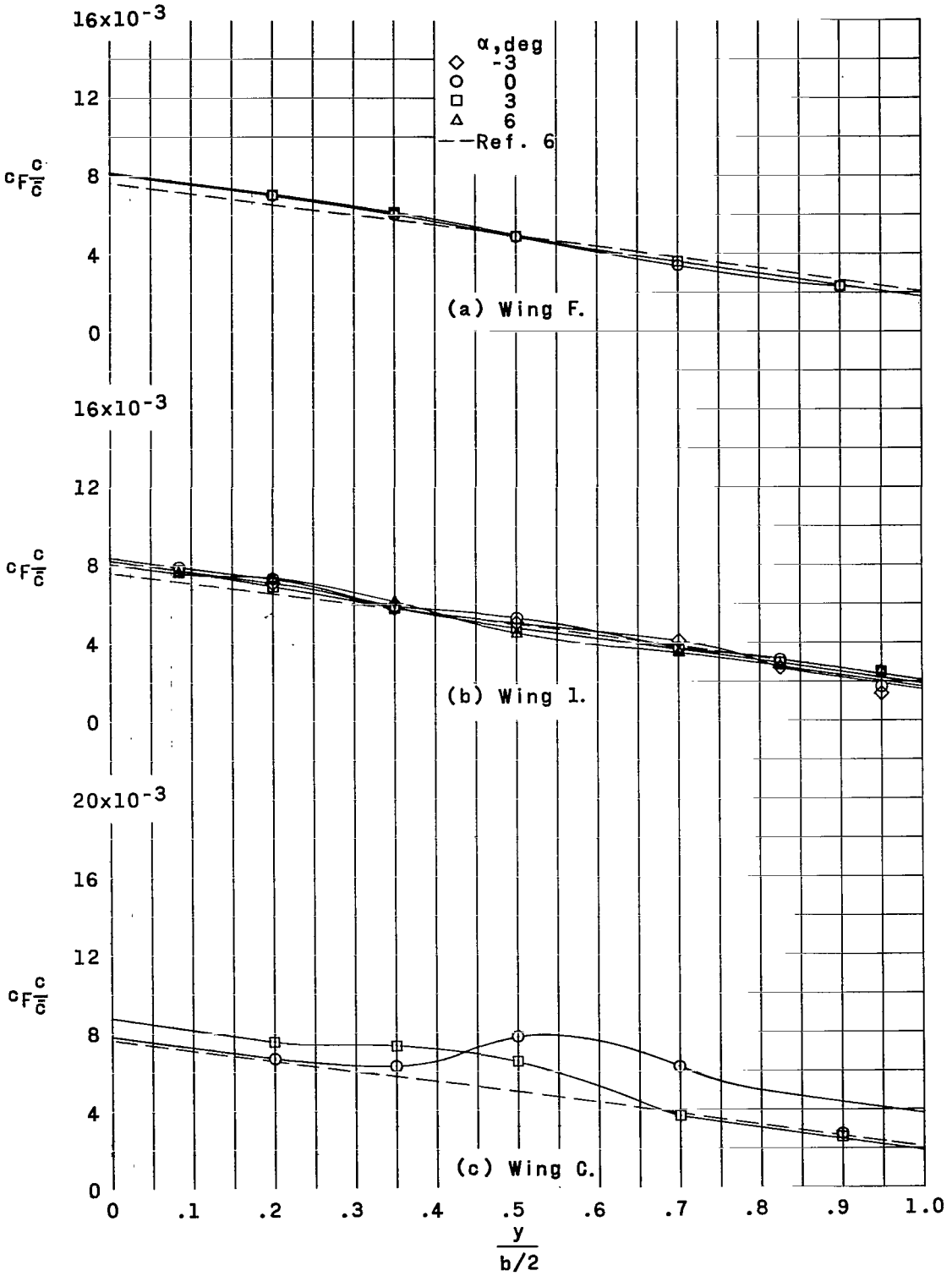

Figure 6.- Variation of section skin-friction coefficient based on $\bar{c}$ with semispan station. M = 2.01.

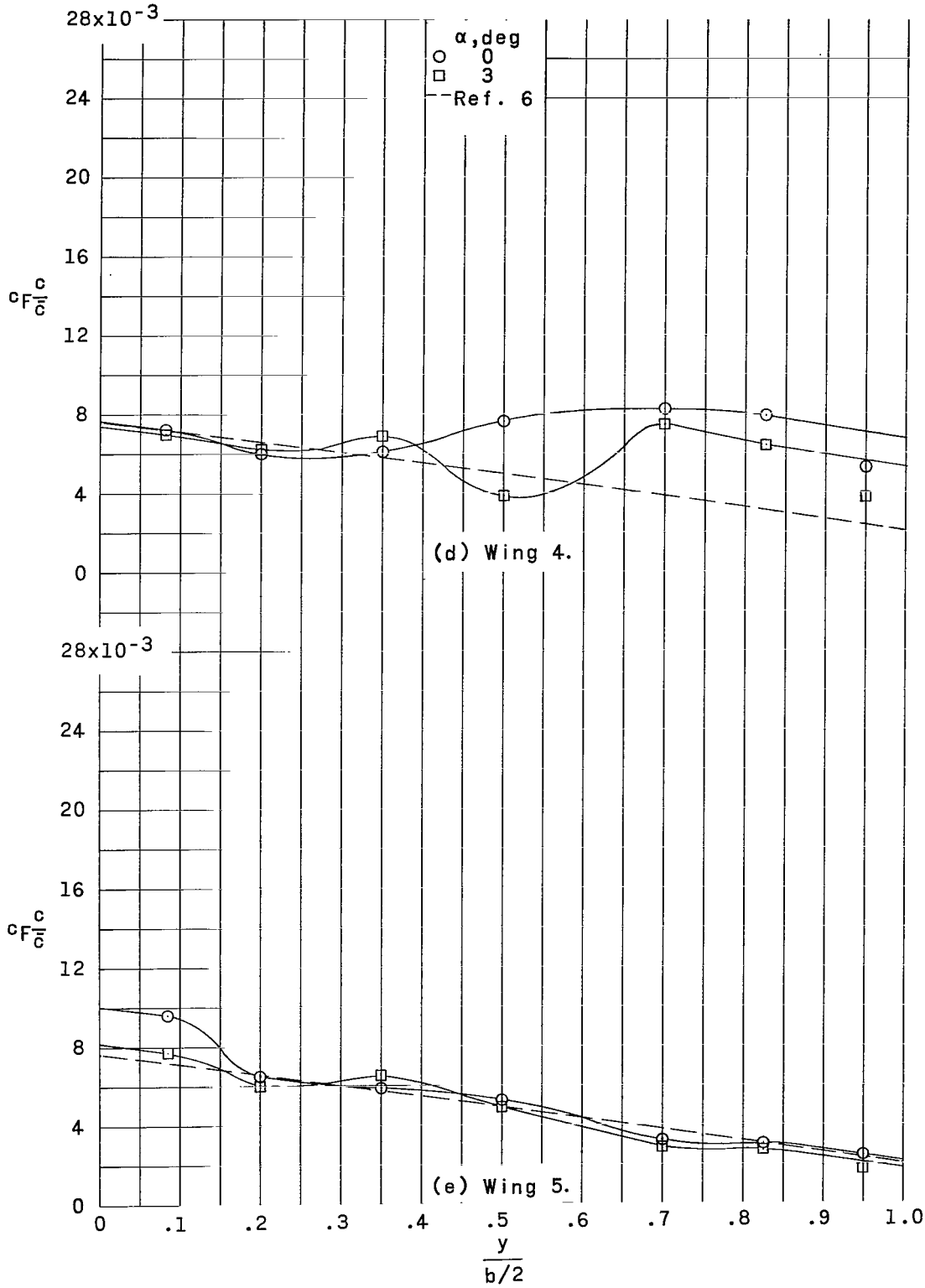

Figure 6.- Concluded.

number (calculated from the pressure coefficients given in ref. 8) on the upper surface normal to the trailing edge and for the given angle of recompression at $\alpha = 6^{\circ}$. The angle of recompression includes the angle of attack and the wing thickness half-angle. No data were taken for wing F at Mach number 2.01 and $\alpha = 6^{\circ}$. There does not appear to be any consistent variation of skin-friction coefficient with angle of attack for wing F (fig. 6(a)), although there are the separation effects at a Mach number of 1.61 and $\alpha = 6^{\circ}$ (fig. 5(a)).

Wing 1.- The measured skin-friction values for wing 1 are slightly above those determined from theory. (See figs. 5(b) and 6(b).) Again, there is a tendency for the skin-friction values to exceed the theory by a greater percentage at the inboard stations than at the outboard stations, just as for wing F. The previously mentioned separation effects at Mach number 1.61 and $\alpha = 6^{\circ}$ are also seen on wing 1 at the inboard stations where the twist in the wing has not appreciably decreased the angle of recompression. Again, as for wing F, there does not appear to be any consistent variation of skin-friction coefficient with angle of attack, although there are separation effects at Mach number 1.61 and $\alpha = 6^{\circ}$.

Wing C and wing 4.- The data for wing C and wing 4 at both Mach numbers tend to be below theory at the inboard stations and considerably above theory at the outboard stations. (See figs. 5(c), 5(d), 6(c), and 6(d).) However, it is known from previous pressure data on these wings (ref. 8) that separation occurs over the outboard portion of the span and that greater momentum losses can be expected. Some typical effects of separation can be seen in figure 4 by comparing the profile taken in an unseparated region (fig. 4(b)) with the profiles taken in separated regions (figs. 4(c) and 4(d)). The increased total-pressure losses due to separation are apparent and the static pressure can also be seen to vary in the vertical direction in the two separated cases. This is typical of many of the profiles taken which show separation losses, but the static pressure generally did not vary appreciably where there was no apparent separation. The fact that the static pressure varies in the vertical direction suggests that the assumption discussed in appendix A, that a straight line can be drawn from δ_l to δ_u to obtain the M_{W+A} profile, is somewhat inaccurate for these cases. Thus, it appears that if a high order of accuracy is to be obtained in measuring the skin-friction values and/or separation momentum losses, wake surveys should be taken far enough downstream of the model to insure that the static pressure will be essentially constant through the wake in the vertical direction at the spanwise station being surveyed.

A possible explanation for the fact that there are data points below theory at the inboard stations of wing C and wing 4 is that the separated area on the wing is bleeding off the adjacent boundary layer and thus the momentum loss in that region is shifted in a spanwise direction toward the separated region. At the outboard stations, the skin-friction data at $\alpha = 0^{\circ}$ are consistently higher than those at $\alpha = 3^{\circ}$ for both Mach

numbers. This fact indicates that at $\alpha = 0^{o}$ the flow is separating on the undersurface of the wing at the leading edge because of the camber, which creates a large negative angle of attack at the leading edge. Consequently, at $\alpha = 3^{o}$, the negative angle of attack at the leading edge is decreased and the separation is decreased.

Wing 5.- Skin-friction values for wing 5 are considerably higher than theory over portions of the span at Mach number 1.61, but at Mach number 2.01 the data were generally on a level with theory. (See figs. 5(e) and 6(e).) The total-pressure profiles suggest that there was a significant amount of separation for Mach number 1.61 at station 6, $\alpha = 0^{o}$ and at station 4, $\alpha = 3^{o}$ and for Mach number 2.01 at station 1, $\alpha = 0^{o}$, since these profiles were not symmetrical.

Skin-friction coefficients (based on local chord).- The data for all wings are presented in another form in figures 7 and 8 where the experimental section skin-friction coefficients based on local chord are plotted against Reynolds number based on local chord for a constant angle of attack. In general, wing 4 appears to have the greatest amount of separation losses at both Mach numbers and the extent and magnitude of separation on all five wings seem to be less at Mach number 2.01 (fig. 8) than at Mach number 1.61 (fig. 7).

Average Wing Skin-Friction Coefficients

The data and the theory curves in figures 5 and 6 were integrated to obtain average skin-friction coefficients based on $\overline{c}$ for the five semispan wings at various angles of attack. These results are presented in table 2 together with the percentage by which the data exceed the theory. The arc length on these wings was found to be only 0.3 percent longer than the chord; therefore, this factor could not have contributed significantly to the increase over theory.

TABLE 2.- AVERAGE SEMISPAN SKIN-FRICTION COEFFICIENT

(a) M = 1.61

Wing	α, deg	C_F	Percentage above theory
F	0	0.00576	6.85
	3	.00579	7.40
	6	.00621	15.20
1	-3	.00590	9.45
	0	.00605	12.23
	3	.00600	11.30
	6	.00627	16.31
C	0	.00991	83.83
	3	.00851	57.86
4	0	.00999	85.31
	3	.00853	58.23
5	0	.00721	33.75
	3	.00639	18.53

(b) M = 2.01

Wing	α, deg	C_F	Percentage above theory
F	0	0.00493	0.16
	3	.00504	2.42
1	-3	.00508	3.23
	0	.00525	6.63
	3	.00500	1.45
	6	.00496	.64
C	0	.00637	29.28
	3	.00566	14.88
4	0	.00720	46.11
	3	.00607	23.30
5	0	.00524	6.31
	3	.00480	-2.42

Since the data for the unseparated cases (wing F and wing 1 at $\alpha = 0^{\circ}$ and 3°) were only slightly above theory, the boundary layer must be fully turbulent and therefore the method of fixing transition used in this investigation appears to be adequate.

Effect of Downstream Measuring Position

One question that arises in momentum surveys is how far downstream of the model should the surveys be made. The choice of the downstream measuring position can affect the accuracy of the measurements, but there should be a relatively large range of downstream positions where the accuracy will not be affected. If the survey is made too close to the wing, the survey will intersect the trailing-edge shock, or the static pressure might not be constant through the wake. If the survey is made too far downstream, there might be large spanwise momentum transfers due to sidewash or the spanwise momentum gradient so that the measured skin-friction values cannot be related to the particular spanwise station surveyed; or, the wake might spread so far that the Mach number losses would be too small to be measured accurately.

The wake was surveyed at various downstream positions behind station 2 to determine the effect of downstream positioning of the rake on the measurement of section skin-friction coefficients. The results are presented in figure 9 where the downstream position is given in percent of the local chord from the trailing edge of the wing. The downstream values of skin-friction coefficient for wing F and wing 1 do not vary appreciably at either Mach number, whereas values for the cambered wings vary considerably with downstream measuring position. However, the cambered wings have substantial regions of separated flow and it is believed that the large spanwise momentum gradients, which result primarily from the fact that only the outboard stations are separated, caused spanwise momentum transfers and consequently the measured skin friction varies with downstream measuring position. The sidewash due to the lift distribution was calculated by the method outlined in reference 11 behind wing C at station 2, $\alpha = 0^{\circ}$, for Mach numbers 1.61 and 2.01 at the 40-percent-chord downstream position and was found to be less than 0.6 ft/sec (0.18 m/sec) for both Mach numbers. This value would not be great enough to cause the large momentum shifts indicated in figure 9.

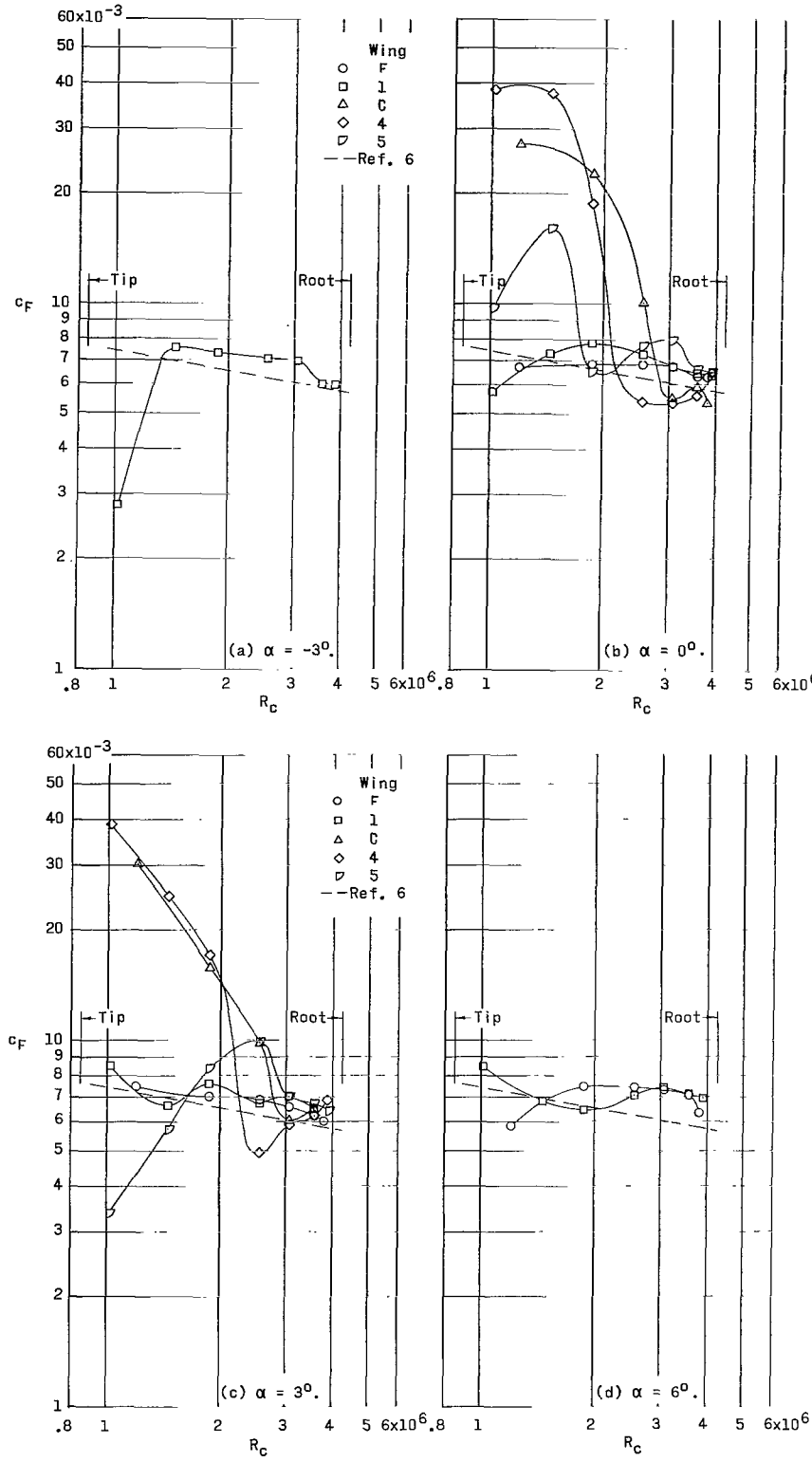

Figure 7.- Variation of section skin-friction coefficient with Reynolds number for constant angle of attack. M = 1.61.

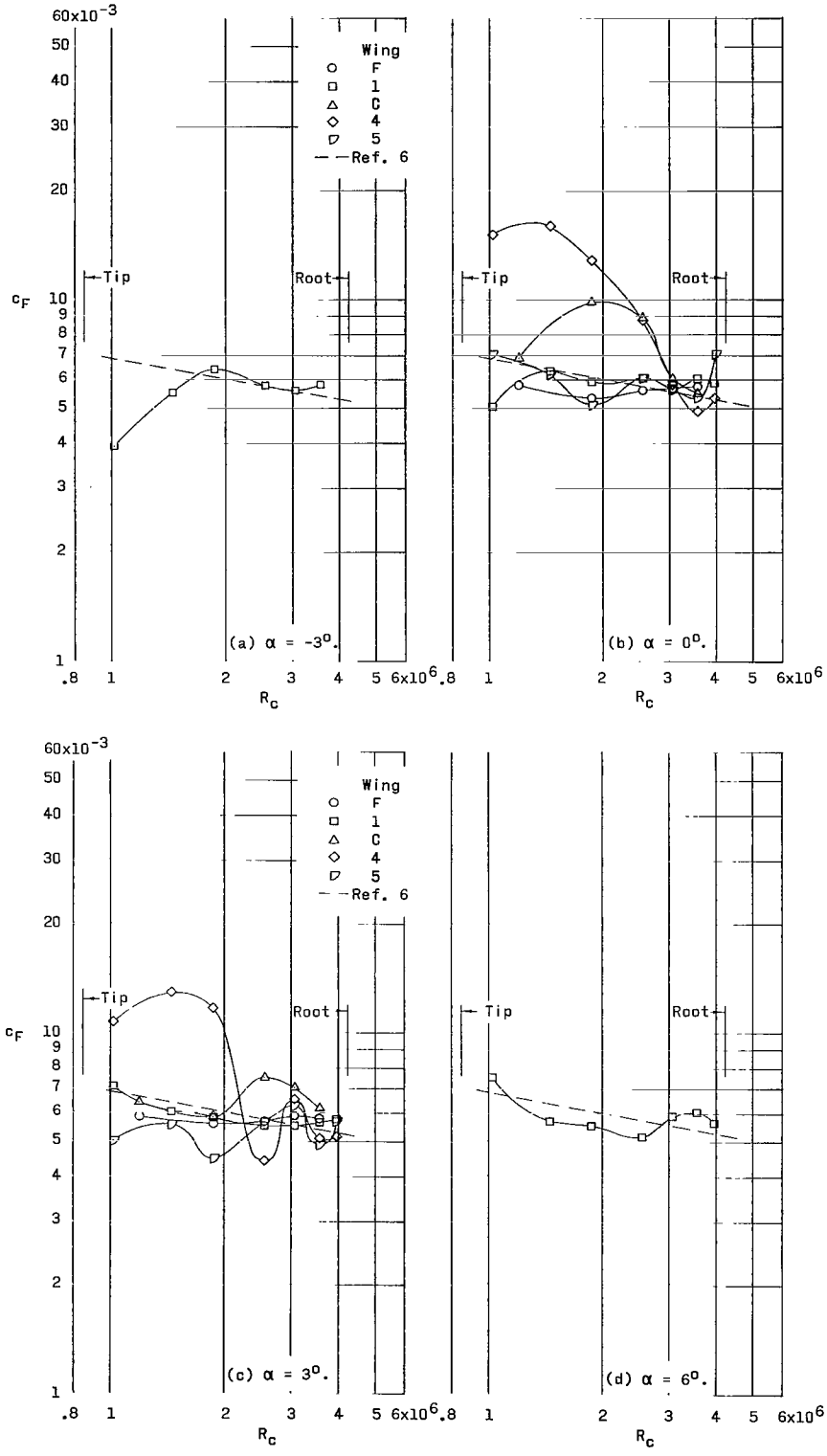

Figure 8.- Variation of section skin-friction coefficient with Reynolds number for constant angle of attack. M = 2.01.

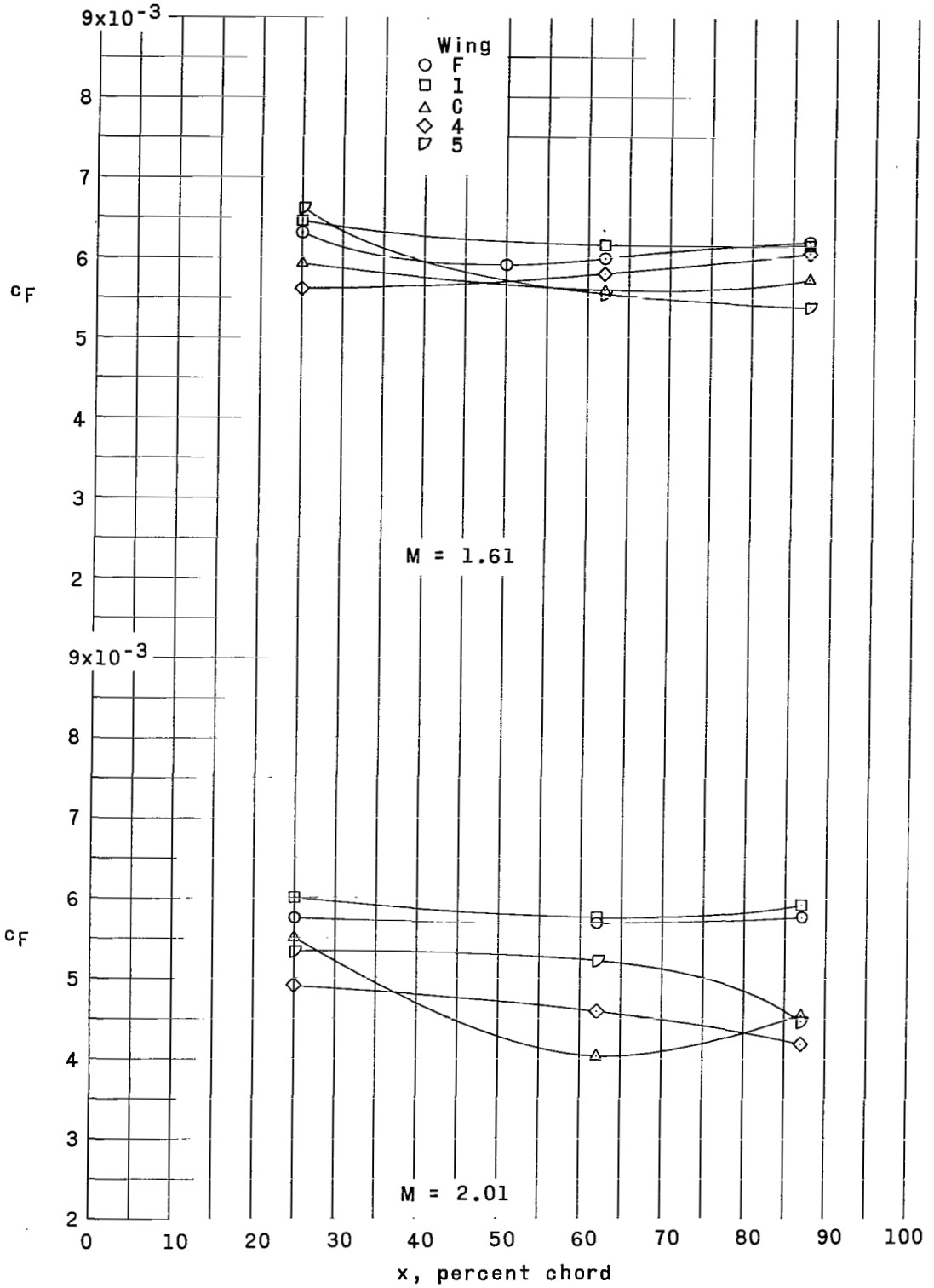

Figure 9.- Effect of distance behind wing on the measurement of section skin-friction coefficient at station 2. $\alpha = 0^{0}$.

CONCLUDING REMARKS

Momentum surveys were made in the wakes behind five swept wings employing various amounts of twist and camber at Mach numbers 1.61 and 2.01 to test the applicability of the wake-survey technique in the measurement of the turbulent three-dimensional boundary-layer skin friction on a wing.

The results indicate that wake surveys can measure the viscous and separation momentum losses incurred by a swept wing with reasonable accuracy and that the viscous momentum losses can be related to section skin-friction coefficient with reasonable accuracy except when there is an appreciable amount of separation on the wing. It appears that for a high order of accuracy to be obtained, wake surveys should be taken far enough downstream of the model to insure that the static pressure will be essentially constant through the wake in the vertical direction at the particular spanwise station being surveyed. The integrated skin-friction values over the span are slightly greater than the integrated values from theory for the wings which had little or no flow separation; but the cambered wings, for which considerable amounts of separation occurred, indicate values much greater than those obtained from theory.

Langley Research Center,
National Aeronautics and Space Administration,
Langley Station, Hampton, Va., August 30, 1966,
720-01-00-04-23.

APPENDIX A

DERIVATION AND DISCUSSION OF EQUATIONS FOR CALCULATION OF SECTION SKIN-FRICTION COEFFICIENTS

The section skin-friction coefficients were calculated from the equation

$$c_F = \frac{2\theta_F}{c} \tag{A1}$$

where θ_F is the two-dimensional momentum thickness due to skin-friction losses. The general expression for the two-dimensional wake momentum thickness is given by

$$\theta = \int_{\delta_l}^{\delta_u} \frac{\rho u}{\rho_\infty u_\infty}\left(1 - \frac{u}{u_\infty}\right)dz \tag{A2}$$

However, as illustrated in figure 10, the local conditions at δ_l and/or δ_u often do not match free-stream conditions. Consequently, equation (A2) is inadequate for calculating the momentum thickness due to skin-friction losses (shown as the hatched areas in fig. 10) since it not only includes the momentum thickness due to skin friction but also the momentum thickness due to wave drag as well as any momentum thickness change which might occur due to any acceleration of the wake with respect to free-stream conditions. Figure 10(a) is typical of the profiles where the Mach number at the outer edges of the skin-friction wake is less than free-stream Mach number, and figure 10(b) is typical of the profiles where the Mach number at the outer edges of the skin-friction wake is greater than free-stream Mach number. Although the total- and static-pressure profiles were dealt with in reducing the data, Mach number profiles are shown in figure 10 since they provide a better illustration of the acceleration effects. The heavy line is the actual Mach number profile calculated from the measured static and total pressures. The free-stream Mach number level is indicated by the straight vertical line, and the upper and lower limits of the skin-friction wake are indicated as δ_u and δ_l, respectively. The M_{W+A} line is the assumed Mach number profile which results from just the wave-drag and flow-acceleration effects. The portion of the M_{W+A} line between δ_l and δ_u defines the local reference conditions of the skin-friction wake and consequently separates the skin-friction losses from the wave-drag and acceleration effects and it was formed by drawing a straight line from δ_l to δ_u. In actual practice the straight line between δ_l and δ_u was drawn on the $p_{t,2}$ profiles, but it will be approximately a straight line on the Mach number profiles also. (The validity of assuming this linear variation of the local reference conditions is discussed in appendix B.) Therefore, the combined effect of the wave drag and any flow acceleration is shown approximately as the cross-hatched areas in figure 10.

The differences between the free-stream Mach number and the Mach number at δ_l and/or δ_u were not random differences but were such that the Mach number at δ_l and/or δ_u is below free-stream Mach number at the inboard stations of the wing and gradually increases to values greater than the free-stream Mach number at the outboard stations. This increase in Mach number at the outboard stations was apparently associated with the tendency for the static pressure on the wing surface to decrease with increasing $\frac{y}{b/2}$ (ref. 8) and with the persistence of this effect being continued downstream. The static-pressure profiles through the wake of wing C shown in figures 4(b), 4(c), and 4(d) are examples of the spanwise variation in static pressure. One explanation for this phenomenon is that it results from the conical nature of the flow past a swept wing.

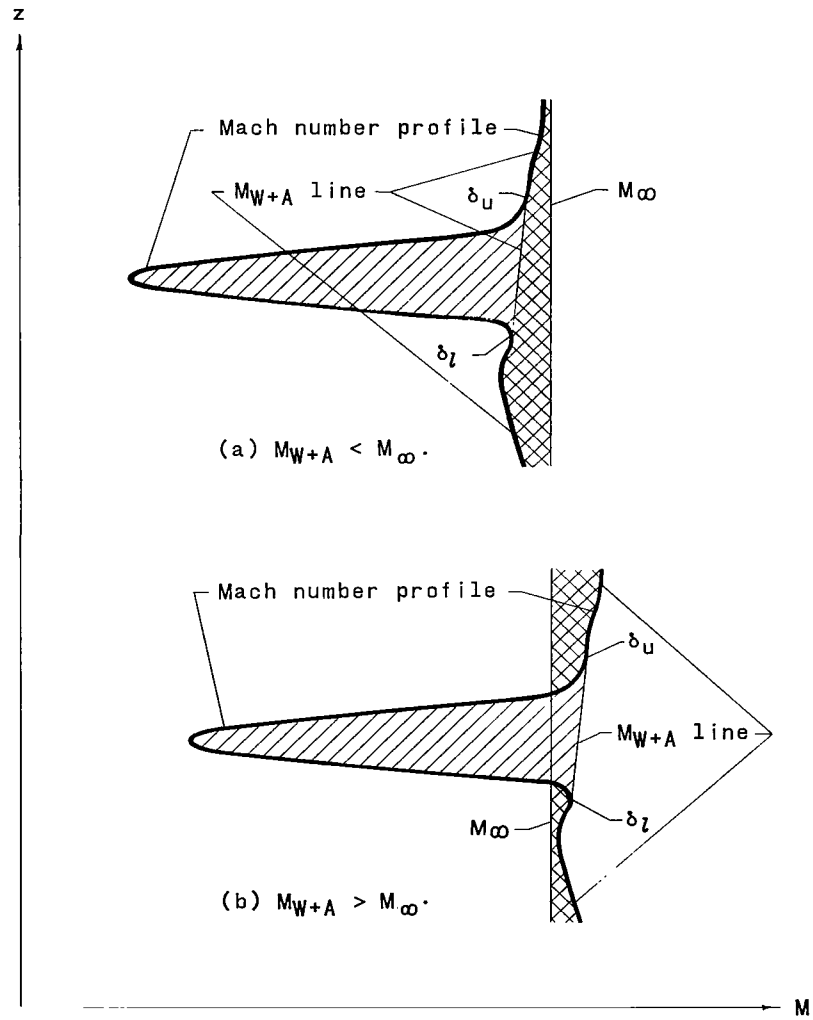

Figure 10.- Sample Mach number profiles illustrating the breakdown of the profile.

It is apparent from the hatched areas in figure 10 that the drag or rate of momentum loss due to skin friction must be determined from the local conditions as follows:

$$\text{Drag} = \int_{\delta_l}^{\delta_u} \rho u \left(u_{W+A} - u\right) dz \tag{A3}$$

Referencing this momentum loss to free stream gives the corresponding momentum thickness

$$\theta_F = \int_{\delta_l}^{\delta_u} \frac{\rho u \left(u_{W+A} - u\right)}{\rho_\infty u_\infty^2} dz = \int_{\delta_l}^{\delta_u} \frac{\rho u}{\rho_\infty u_\infty} \left(\frac{u_{W+A}}{u_\infty} - \frac{u}{u_\infty}\right) dz \tag{A4}$$

or

$$\theta_F = \int_{\delta_l}^{\delta_u} \frac{\rho u}{\rho_\infty u_\infty} \left(1 - \frac{u}{u_\infty}\right) dz - \int_{\delta_l}^{\delta_u} \frac{\rho u}{\rho_\infty u_\infty} \left(1 - \frac{u_{W+A}}{u_\infty}\right) dz \tag{A5}$$

The first term on the right-hand side of equation (A5) is the general expression for θ defined in equation (A2); the second term represents the momentum thickness due to the combined effect of wave drag and acceleration, which can be defined as θ_{W+A}. The expression for θ_F is thus

$$\theta_F = \theta - \theta_{W+A} \tag{A6}$$

Applying the transformation derived in appendix C to equation (A5) leads to

$$\theta_F = \sum_{\delta_l}^{\delta_u} \frac{pM}{p_\infty M_\infty} \left(\sqrt{\frac{1 + \frac{\gamma - 1}{2} M^2}{1 + \frac{\gamma - 1}{2} M_\infty^2}} - \frac{M}{M_\infty} \right) \Delta z$$

$$- \sum_{\delta_l}^{\delta_u} \frac{pM}{p_\infty M_\infty} \left(\sqrt{\frac{1 + \frac{\gamma - 1}{2} M^2}{1 + \frac{\gamma - 1}{2} M_\infty^2}} - \frac{M_{W+A}}{M_\infty} \sqrt{\frac{1 + \frac{\gamma - 1}{2} M^2}{1 + \frac{\gamma - 1}{2} M_{W+A}^2}} \right) \Delta z \tag{A7}$$

where M_{W+A} is a function of z.

APPENDIX B

DISCUSSION OF POSSIBLE ERRORS INVOLVED WITH WAKE SURVEYS

An accurate quantitative estimate of the possible magnitude of errors that may be involved in the method used to reduce wake surveys to boundary-layer skin friction is difficult to make because it requires a knowledge of the characteristics of boundary-layer growth over the wing, the characteristics of the transition of the wing boundary layer to a wake at the foot of the trailing-edge shock, and the spreading of the wake downstream of the wing. In particular, there is insufficient knowledge of the last two items for supersonic flow. A few qualitative remarks, however, can be made.

Equation (A3) of appendix A neglects a term involving the difference in local static pressure from free-stream static pressure. Inasmuch as the static-pressure differences between the measuring stations and free stream were small, the magnitude of the error in neglecting this effect is estimated to be small. This belief is supported by the results of surveys at different downstream stations, which showed only small variation in the estimated skin-friction drag when the flow over the wing was not separated.

In this paper the reference velocity u_{W+A} is found by assuming that the total pressure $p_{t,2}$ varies linearly across the viscous wake and the linear variation is inferred from the values of the total pressure just outside the viscous wake. This procedure is of course approximate and may be expected to introduce some error. In particular, because the strength of the trailing-edge shock decreases as it penetrates the lower velocity regions of the wake, the correct values of u_{W+A} may generally be greater than estimated, but this effect is partly counterbalanced by the increased strength of the leading-edge shock wave as it bends around the wing leading edge. The error arising from an inaccurate estimate of the reference velocity across the skin-friction wake is also believed to be small since the estimated skin-friction drag varied only slightly with angle of attack so long as the flow did not separate, whereas the shock-wave system changed considerably.

APPENDIX C

TRANSFORMATION OF INTEGRAL FORM OF EQUATIONS θ AND θ_{W+A} TO SUMMATION FORM

The general expression for the two-dimensional momentum thickness measured in the wake behind a wing is given by

$$\theta = \int_{\delta_l}^{\delta_u} \frac{\rho u}{\rho_\infty u_\infty}\left(1 - \frac{u}{u_\infty}\right)dz \tag{C1}$$

However, if θ is expressed in terms of Mach number and pressure, it can be calculated more directly from the measured static- and total-pressure profiles.

The ratio of the temperature to the total temperature is given by the expression

$$\frac{T}{T_t} = \left(1 + \frac{\gamma - 1}{2}M^2\right)^{-1} \tag{C2}$$

It was assumed that the total temperature was constant throughout the wake and equal to free-stream total temperature; consequently on substituting equation (C2) into the equation of state

$$\frac{\rho}{\rho_\infty} = \frac{p}{p_\infty}\frac{T_\infty}{T} \tag{C3}$$

gives

$$\frac{\rho}{\rho_\infty} = \frac{p}{p_\infty}\left(\frac{1 + \frac{\gamma - 1}{2}M^2}{1 + \frac{\gamma - 1}{2}M_\infty{}^2}\right) \tag{C4}$$

From the definition of Mach number,

$$M = \frac{u}{a} \tag{C5}$$

the velocity ratio can be expressed as

$$\frac{u}{u_\infty} = \frac{M}{M_\infty}\frac{a/a_t}{a_\infty/a_t} \tag{C6}$$

The equation for the ratio of the speed of sound to the speed of sound at stagnation conditions is given by

$$\frac{a}{a_t} = \left(1 + \frac{\gamma - 1}{2}M^2\right)^{-1/2} \tag{C7}$$

Substituting equation (C7) into equation (C6) gives

$$\frac{u}{u_\infty} = \frac{M}{M_\infty}\sqrt{\frac{1 + \frac{\gamma - 1}{2}M_\infty^2}{1 + \frac{\gamma - 1}{2}M^2}} \tag{C8}$$

Substituting equations (C4) and (C8) into equation (C1) and employing the step integration method transforms the integral form of the equation for θ to the following summation form:

$$\theta = \sum_{\delta_l}^{\delta_u} \frac{pM}{p_\infty M_\infty}\left(\sqrt{\frac{1 + \frac{\gamma - 1}{2}M^2}{1 + \frac{\gamma - 1}{2}M_\infty^2}} - \frac{M}{M_\infty}\right)\Delta z \tag{C9}$$

Similarly, θ_{W+A}, expressed in integral form as

$$\theta_{W+A} = \int_{\delta_l}^{\delta_u} \frac{\rho u}{\rho_\infty u_\infty}\left(1 - \frac{u_{W+A}}{u_\infty}\right)dz \tag{C10}$$

is given by

$$\theta_{W+A} = \sum_{\delta_l}^{\delta_u} \frac{pM}{p_\infty M_\infty}\left(\sqrt{\frac{1 + \frac{\gamma - 1}{2}M^2}{1 + \frac{\gamma - 1}{2}M_\infty^2}} - \frac{M_{W+A}}{M_\infty}\sqrt{\frac{1 + \frac{\gamma - 1}{2}M^2}{1 + \frac{\gamma - 1}{2}M_{W+A}^2}}\right)\Delta z \tag{C11}$$

where M_{W+A} is a function of z.

REFERENCES

1. Adcock, Jerry B.; Peterson, John B., Jr.; and McRee, Donald I.: Experimental Investigation of a Turbulent Boundary Layer at Mach 6, High Reynolds Numbers, and Zero Heat Transfer. NASA TN D-2907, 1965.

2. Chapman, Dean R.; and Kester, Robert H.: Turbulent Boundary-Layer and Skin-Friction Measurements in Axial Flow Along Cylinders at Mach Numbers Between 0.5 and 3.6. NACA TN 3097, 1954.

3. Czarnecki, K. R.; and Monta, William J.: Boundary-Layer Velocity Profiles and Skin Friction Due to Surface Roughness on an Ogive Cylinder at Mach Numbers of 1.61 and 2.01. NASA TN D-2048, 1963.

4. Patterson, Elizabeth W.; and Braslow, Albert L.: Ordinates and Theoretical Pressure-Distribution Data for NACA 6- and 6A-Series Airfoil Sections With Thickness From 2 to 21 and From 2 to 15 Percent Chord, Respectively. NASA TR R-84, 1961. (Supersedes NACA TN 4322.)

5. Abbott, Ira H.; Von Doenhoff, Albert E.; and Stivers, Louis S., Jr.: Summary of Airfoil Data. NACA Rept. 824, 1945. (Supersedes NACA WR L-560.)

6. Sommer, Simon C.; and Short, Barbara J.: Free-Flight Measurements of Turbulent-Boundary-Layer Skin Friction in the Presence of Severe Aerodynamic Heating at Mach Numbers From 2.8 to 7.0. NACA TN 3391, 1955.

7. Nielsen, Jack N.: Missile Aerodynamics. McGraw-Hill Book Co., Inc., 1960.

8. Landrum, Emma Jean: A Tabulation of Wind-Tunnel Pressure Data and Section Aerodynamic Characteristics at Mach Numbers of 1.61 and 2.01 for a Reflex Cambered Wing and a Cambered and Twisted Wing Having the Same Swept Planform. NASA TN D-1393, 1962.

9. Lord, Douglas R.; and Czarnecki, K. R.: Pressure Distributions and Aerodynamic Characteristics of Several Spoiler-Type Controls on a Trapezoidal Wing at Mach Numbers of 1.61 and 2.01. NACA RM L56E22, 1956.

10. Reshotko, Eli, and Tucker, Maurice: Effect of a Discontinuity on Turbulent Boundary-Layer-Thickness Parameters With Application to Shock-Induced Separation. NACA TN 3454, 1955.

11. Bobbitt, Percy J.: Tables for the Rapid Estimation of Downwash and Sidewash Behind Wings Performing Various Motions at Supersonic Speeds. NASA MEMO 2-20-59L, 1959.

"The aeronautical and space activities of the United States shall be conducted so as to contribute . . . to the expansion of human knowledge of phenomena in the atmosphere and space. The Administration shall provide for the widest practicable and appropriate dissemination of information concerning its activities and the results thereof."

—NATIONAL AERONAUTICS AND SPACE ACT OF 1958

NASA SCIENTIFIC AND TECHNICAL PUBLICATIONS

TECHNICAL REPORTS: Scientific and technical information considered important, complete, and a lasting contribution to existing knowledge.

TECHNICAL NOTES: Information less broad in scope but nevertheless of importance as a contribution to existing knowledge.

TECHNICAL MEMORANDUMS: Information receiving limited distribution because of preliminary data, security classification, or other reasons.

CONTRACTOR REPORTS: Technical information generated in connection with a NASA contract or grant and released under NASA auspices.

TECHNICAL TRANSLATIONS: Information published in a foreign language considered to merit NASA distribution in English.

TECHNICAL REPRINTS: Information derived from NASA activities and initially published in the form of journal articles.

SPECIAL PUBLICATIONS: Information derived from or of value to NASA activities but not necessarily reporting the results of individual NASA-programmed scientific efforts. Publications include conference proceedings, monographs, data compilations, handbooks, sourcebooks, and special bibliographies.

Details on the availability of these publications may be obtained from:

SCIENTIFIC AND TECHNICAL INFORMATION DIVISION

NATIONAL AERONAUTICS AND SPACE ADMINISTRATION

Washington, D.C. 20546